Differential Pilots Aided In-Band OSNR Monitor with Large Nonlinear Tolerance

Liang Dou[1], Zhenning Tao[1], Ying Zhao[1], Shoichiro Oda[2], Yasuhiko Aoki[2], Takeshi Hoshida[3], Jens C. Rasmussen[2]

1) Fujitsu R&D Center, No. 56 Dongsihuan Zhong Road, Beijing, 100025, China

2) Fujitsu Laboratories Ltd., 3) Fujitsu Limited, 1-1 Kamikodanaka 4-chome, Nakahara-ku, Kawasaki, 211-8588, Japan

Abstract: Differential pilots aided in-band OSNR monitor is proposed and verified under 32GBaud WDM experiments. High accuracy (<0.5dB error), no dependency on pulse shapes, and large nonlinear tolerance (1dB error after 4dBm 2700km transmission) are proved.

OCIS codes: (060.2360) Fiber optics links and subsystems; (060.4370) Nonlinear optics, fibers

1. Introduction

In-band optical signal to noise ratio (OSNR) is a quantitative value to indicate the amplified spontaneous noise (ASE) along the link and it can provide a good guidance for optical network design, e.g. wavelength assignment or modulation adaption [1]. After passing through the optical link, the received signal is distorted and mixed with all kinds of noise. How to separate the signal and ASE noise from other distortions is the key to obtain OSNR. Most conventional OSNR monitors are only applicable for specific scenarios. Spectral analysis is valid for system with large channel spacing and no optical filters [2], and it cannot be applied for the high spectral efficiency systems. Polarization nulling technique is also an efficient way, but it is limited to the single polarization system [3]. With the help of coherent receiver and digital signal processing (DSP), error vector magnitude (EVM) is proved to be an appropriate metric to measure OSNR [4]. By adding pilot at transmitter side, OSNR can be measured by Fourier analysis at receiver side in an effective way [5]. However, for the long haul transmission systems, OSNR value would be underestimated due to the existence of nonlinear noise induced by Kerr effect. In [6], the intra-channel nonlinear noise is excluded from the total noise with empirical correction based on their different auto-correlation properties.

In this paper, an accurate in-band OSNR monitor is proposed with assistance of differential pilot sequences at transmitter side. With such pilot design, ASE noise can be separated from other nonlinear noise. At B2B conditions, 0.5dB accuracy is experimentally verified for both NRZ and Nyquist pulse shapes. Both intra-channel and inter-channel nonlinearity tolerances are also investigated under 9 channel WDM loop experiments.

2. Differential Pilots Aided OSNR Monitor

The frame structure of the transmitted signal is shown in Fig. 1(a). Each frame is composed by pilot and payload. Generally, the pilot can be realized by a series of phase modulated symbols with constant phase interval. To be compatible with the following payload symbols, one possible realization of pilot sequence is to generate QPSK constellation points in both clockwise and counter-clockwise directions for *H* and *V* polarizations. As Fig. 1(a) shows, the period of pilot sequence is 4 symbols, so that the pilot frequency is equal to positive or negative 1/4 of the baudrate depending on the direction.

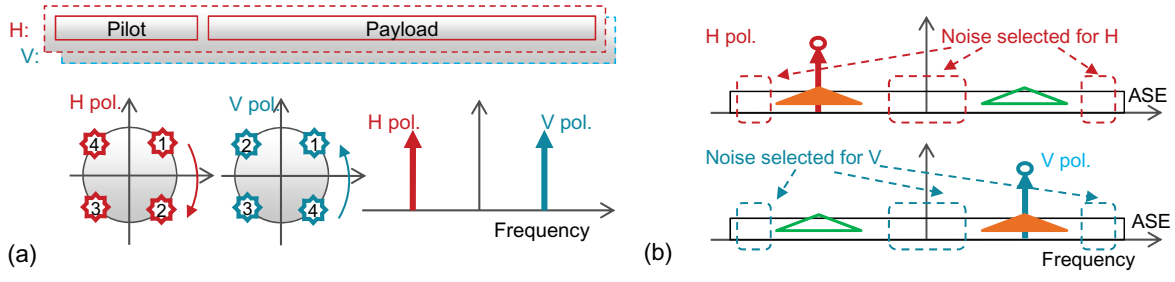

Fig. 1(a): Frame structure with differential pilots. (b): Noise calculation area for two polarizations by considering intra-channel nonlinear noise (circle), inter-channel nonlinear phase noise (filled triangle) and polarization crosstalk (hollow triangle).

Since the OSNR value changes in low speed, the OSNR monitor is realized by off-line processing based on the snapshot of received signal. After equalization, the two polarization signal at pilot period is converted to frequency domain, as shown in Fig. 1(b). In linear transmission regime, the spectrum is composed by one single spectrum

component which denotes pilot and a flat pedestal which is ASE noise. Due to their significant difference in frequency domain, the noise spectrum density can be measured by the spectrum components different from dedicated pilot frequencies. Together with the total power of the equalized payload, OSNR value can be achieved.

As the launch power increasing, nonlinear noise cannot be ignored. For intra-channel nonlinearity, the perturbation nonlinear model depicts that the nonlinear noise for H polarization at time slot of k symbol is the summation of three symbols products $H_{m+k}H_{n+k}H_{m+n+k}$* and $H_{m+k}V_{n+k}V_{m+n+k}$*, where H/V denotes symbol information of two polarizations and $m/n/k$ is the integer index of sending symbols [8]. If the pilot is considered as $e^{j\omega kT}$ and $e^{-j\omega kT}$, where ω means frequency, the resulted three symbols products on k time slot are $e^{j\omega kT}$ and $e^{j\omega 2mT}e^{j\omega kT}$. Although there is an additional coefficient in front of three symbols products coming from orthogonal polarization, it still keeps single frequency nature after summation. So the OSNR calculation method keeps the same as that in linear case.

The inter-channel nonlinearity is more complicated comparing with intra-channel nonlinearity. According to the cross phase modulation (XPM) model, it includes two effects, e.g. nonlinear phase noise and polarization crosstalk [9]. The nonlinear phase noise is a multiplicative noise, and it broadens the spectrum of the pilot, which is denoted by the filled triangles in Fig 1(c). The polarization crosstalk on H polarization is considered as field product u_{1v}*u_{2h}*$conj(u_{2v})$ convoluted by a low pass filter determined by the system parameters, where u_{1x} denotes the electrical field of probe signal and u_{2x} is that of pump signal. According to the differential pilot design, the polarization crosstalk appears at the frequency with the opposite sign, shown by the hollow triangle in Fig 1(c). Considering the XPM has low pass filter nature [5], it is necessary to abandon the spectrum region around the two differential pilots and measure the dashed area in Fig. 1(c) to calculate ASE spectral density.

3. Experiment Setup

The WDM loop experiment platform is shown in Fig. 2. Nine narrow line width lasers with 50GHz channel spacing are first combined together and then fed into the optical I/Q modulator, which is driven by a 32Gbaud NRZ/Nyquist source. Here the Nyquist pulse has roll off factor of 0.15. Their corresponding optical eye diagrams are shown in the inset of Fig. 2. The total frame length is 32768 symbols and 256 of them are allocated for pilot. Proper de-correlation scheme is applied [10] to emulate the practical scenario. Before launching into the loop, power equalization among all the 9 channels is applied, and the spectrum of Nyquist WDM is shown in the inset of Fig. 2.

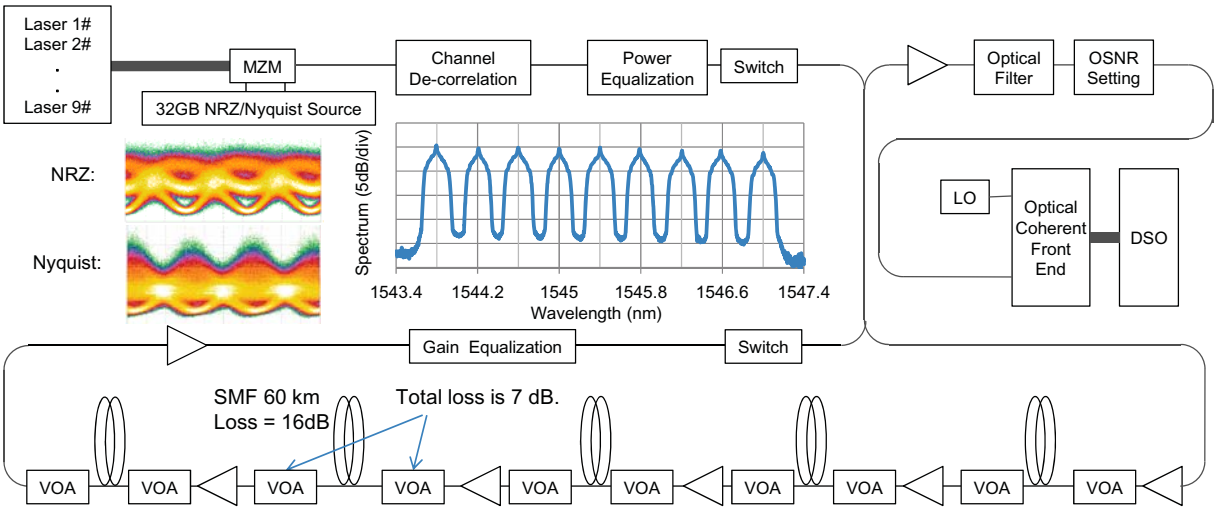

Fig. 2. Experiment setup of WDM loop transmission. VOA: variable optical attenuator. DSO: digital storage oscilloscope. LO: local oscillator.

The transmission loop is composed by five identical spans with a gain equalizer. For each span, there are two variable optical attenuators (VOA), 60km fiber and an erbium doped amplifier (EDFA). The loss of the fiber together with the connectors is around 16dB. The total loss of the two VOAs is fixed to 7dB. By adjusting the quota between the two VOAs, the fiber launch power can be swept from -3dBm to 4dBm without changing the status of EDFA. So that the delivered OSNR after each round of loop is a constant, and the nonlinear tolerance of OSNR monitor can be judged by the variation of the measured results.

After loop transmission, the center channel is filtered out and additional noise is added to control the OSNR value. With local oscillator and optical coherent front end, the optical field can be converted to electrical domain and saved by digital storage oscilloscope (DSO) at 80 GSa/s. In digital domain, the proposed signal processing is performed, and the final OSNR is estimated by averaging the instantaneous OSNR values over 100 times.

4. Experiment Results

The proposed OSNR monitor is first verified under back to back condition. The neighboring channel's lasers are all turned off and the OSNR value is controlled by the noise loading power at the receiver side. Fig. 3(a) compares the estimated OSNR with the pre-set OSNR, which is measured by the optical spectrum analyzer. The estimation error is less than 0.5dB within the OSNR range from 10dB to 25dB and it is also pulse shapes independent. Notice that the electrical noise at both transmitter and receiver side is excluded by considering the measured OSNR without noise loading as a reference. Besides this operation, there is no other artificial fitting parameter during OSNR calculation process.

After B2B accuracy verification, intra-channel nonlinearity tolerance is first investigated by the loop experiment. The lumped ASE at the receiver side is omitted, so that the estimated OSNR should be equal to the delivered OSNR. By setting the attenuation of VOA before the fiber to 7dB and VOA after to 0dB, the launch power reaches the minimum -3dBm. As Fig. 3(b) shows, OSNR is estimated under different distance up to 2700km. Due to the identical ASE noise power for each loop, the delivered OSNR in dB form should agree with common logarithm function multiplied by -10. As shown in the inset of Fig. 3(b), the common logarithm function fitting accuracy R^2 is larger than 0.99 and the coefficient before common logarithm is -9.8, which is very close to -10. So it is reasonable to consider OSNR values with -3dBm as the real delivered OSNR, which is not influenced by nonlinearity. Fig. 3(b) shows a group of curves, and they include the results for both NRZ and Nyquist pulse shapes with different launch power from -3dBm to 4dBm. For all those conditions, the estimation error is within 0.5dB. The inset of Fig. 3(b) shows the comparison of two constellations after 1500km transmission with -3dBm and 4dBm launch power. It can be concluded that pilot sequence is not influenced by nonlinear noise as much as payload be.

The OSNR monitor's performance is finally investigated under the 9 channel WDM transmission experiment with Nyquist pulse shaping. For -3dBm launch power, both high fitting accuracy of common logarithm function and the coefficient of -9.8, listed in the inset of Fig. 3(c), indicate the linear transmission regime. Here, OSNR estimation results based on EVM are also shown in Fig. 3(c) for comparison [4]. At -3dBm launch power, the system noise is governed by ASE, and EVM result shows good agreement with proposed method. By increasing the launch power up to 4dBm, the maximum error of the proposed method is around 1dB. Such error originates from the residual XPM noise which may diffuse into the ASE noise calculation region. On the other hand, large deviations are found for EVM method due to its high sensitivity to nonlinear noise when the launch power is increased to 0dBm or 4dBm.

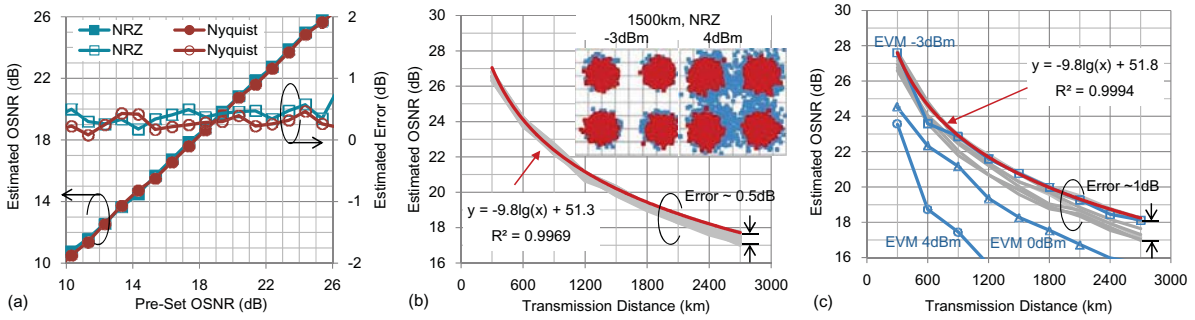

Fig. 3(a): OSNR estimation accuracy at B2B conditions. (b): Estimated OSNR values after single channel transmission experiment. The equations show the common logarithm function fitting result at -3dBm. Gray curves are estimation results for both NRZ and Nyquist, and the launch power is swept from -3dBm to 4dBm. In the constellation plots, red dot denotes pilot and blue dot denotes payload. (c) Estimated OSNR values after WDM transmission experiment. Gray curves are estimation results with launch power changing from -3dBm to 4dBm.

5. Conclusion

An in-band OSNR monitor is proposed based on differential pilot sequence at transmitter side together with DSP algorithms after coherent detection. With such design, the ASE noise can be isolated from intra-channel and inter-channel nonlinear noise in frequency domain. High estimation accuracy together with independence of pulse shapes are verified under B2B experiments. Long distance WDM loop experiment shows large nonlinear tolerance further.

6. Reference

[1] S. J. Savory, Photon. Technol. Lett., Vol. 26, pp 1057-1060, 2014.
[2] D. C. Kilper *et al.*, ECOC2002, paper 7.4.4, 2002.
[3] J. H. Lee *et al.*, J. Lightwave Technol., Vol. 24, pp. 4162-4171, 2006.
[4] R. Schmogrow *et al.*, Photon. Technol. Lett., Vol. 24, 61-63, 2012.
[5] S. Okamoto *et al.*, OECC2013, paper TuR2-4, 2013.
[6] Z. Dong *et al.*, Optical Express, Vol. 20, pp. 19520-19534, 2012.
[7] M. Yan *et al.*, ECOC2013, paperTu.1.E.4, 2013.
[8] L. Dou *et al.*, OFC2011, paper OThF5, 2011.
[9] Z. Tao *et al.*, J. Lightwave Technol. Vol. 29, pp. 974-986, 2011.
[10] Z. Tao *et al.*, ECOC2009, paper 9.4.2, 2009.